JACS
JOURNAL OF THE AMERICAN CHEMICAL SOCIETY

Article

pubs.acs.org/JACS

Terazulene Isomers: Polarity Change of OFETs through Molecular Orbital Distribution Contrast

Yuji Yamaguchi,[†] Maki Takubo,[†] Keisuke Ogawa,[†] Ken-ichi Nakayama,[†] Tomoyuki Koganezawa,[‡] and Hiroshi Katagiri*[,†]

[†]Graduate School of Science and Engineering, Yamagata University, 4-3-16 Jonan, Yonezawa, Yamagata 992-8510, Japan
[‡]Japan Synchrotron Radiation Research Institute (JASRI), SPring-8, 1-1-1 Kouto, Sayo, Hyogo 679-5198, Japan

Supporting Information

ABSTRACT: Intermolecular orbital coupling is fundamentally important to organic semiconductor performance. Recently, we reported that 2,6′:2′,6″-terazulene (**TAz1**) exhibited excellent performance as an n-type organic field-effect transistor (OFET) via molecular orbital distribution control. To validate and develop this concept, here we present three other terazulene regioisomers, which have three azulene molecules connected at the 2- or 6-position along the long axis of the azulene, thus constructing a linear expanded π-conjugation system: 2,2′:6′,2″-terazulene (**TAz2**), 2,2′:6′,6″-terazulene (**TAz3**), and 6,2′:6′,6″-terazulene (**TAz4**). **TAz2** and **TAz3** exhibit ambipolar characteristics; **TAz4** exhibits clear n-type transistor behavior as an OFET. The lowest unoccupied molecular orbitals (LUMOs) of all terazulenes are fully delocalized over the entire molecule. In contrast, the highest occupied molecular orbitals (HOMOs) of **TAz2** and **TAz3** are delocalized over the 2,2′-biazulene units; the HOMOs of **TAz4** are localized at one end of the azulene unit. These findings confirm that terazulene isomers which are simple hydrocarbon compounds are versatile materials with a tunable-polarity FET characteristic that depends on the direction of the azulene unit and the related contrast of the molecular orbital distribution in the terazulene backbone.

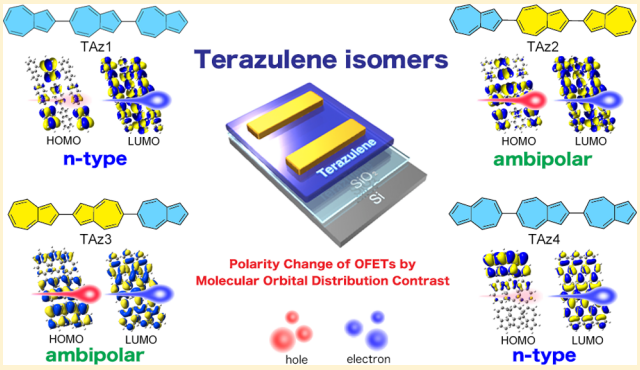

INTRODUCTION

Azulene ($C_{10}H_8$) is a popular molecule in the class of compounds known as nonbenzenoid aromatic hydrocarbons; it has attracted much attention recently because of its unusual properties, typified by a large dipole moment and long-wavelength absorption.[1−3] These features are derived from the nonalternant hydrocarbon character of azulene, and a fundamental difference between it and the alternant hydrocarbon naphthalene arises from differences in their molecular orbital geometries. The highest occupied molecular orbital (HOMO) and the lowest unoccupied molecular orbital (LUMO) of azulene are not mirror-related in orbital geometry; therefore, the absolute values of their atomic orbital coefficients differ substantially. Thus, the energy gap is smaller than anticipated, resulting in a lower transition energy. As a result, the introduction of azulene groups can be used to trigger the construction of π-conjugated materials with a narrow energy gap. To date, azulene-based conjugated compounds have been investigated in various applications, including near-IR absorption materials,[4−6] conducting polymers,[7,8] nonlinear optics,[9−12] fluorescence switching,[13−15] electrochromic materials,[16,17] and organic solar-cell materials.[18−22]

The substitution position of azulene strongly affects the optical properties of azulene-based materials.[23−28] For example, azulene-based compounds substituted at the 2- or 6-position have narrower HOMO−LUMO energy gaps and longer absorption wavelengths than compounds substituted at the 1- or 3-position.[14,29,30] In addition, the 2- and/or 6-substituted azulene oligomers exhibit rectilinear structures with strong intermolecular interactions and high-order orientations in the crystalline state. The π-conjugated molecules with a high-aspect-ratio molecular shape generally prefer a well-defined herringbone packing, as observed in high-performance organic field-effect transistor (OFET) materials such as pentacene and oligothiophene derivatives.[31−34] Azulene has been rarely studied as the building block in OFET materials.[22,35,36] However, recently we developed linear expanded azulene π-conjugation oligomers as OFET materials[37] and reported that an oligomer comprising only azulene units 2,6′:2′,6″-terazulene (**TAz1**) (Figure 1) exhibited excellent n-type transistor performance.[38] The LUMO of **TAz1** is well-distributed over the entire molecule, whereas the HOMO is localized at one end, indicating an advantage of electron carrier transport over hole transport. This asymmetric property between the HOMO and LUMO in **TAz1** is derived from the asymmetric character of the HOMO and LUMO in azulene.

Received: July 6, 2016
Published: August 11, 2016

DOI: 10.1021/jacs.6b06877
J. Am. Chem. Soc. 2016, 138, 11335−11343

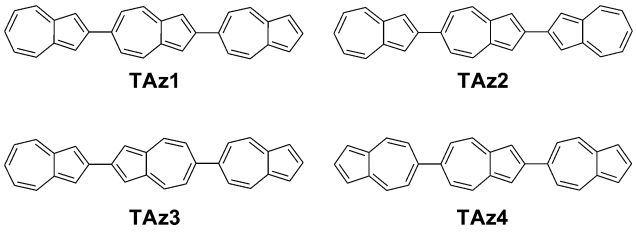

Figure 1. Chemical structure of terazulene isomers.

Terazulene includes four regioisomers [**TAz1**, 2,2′:6′,2″-terazulene (**TAz2**), 2,2′:6′,6″-terazulene (**TAz3**), and 6,2′:6′,6″-terazulene (**TAz4**), Figure 1], each of which is expected to exhibit unique properties, including internal dipole moments and different distributions of their HOMO and LUMO. Herein, we describe the synthesis, structure, and properties of new terazulene isomers (**TAz2**, **TAz3**, and **TAz4**) and specifically focus on their carrier transport properties as evaluated in OFET devices and the dependence of OFET polarity on the molecular orbital distributions.

RESULTS AND DISCUSSION

Synthesis and Thermal Properties. The syntheses of terazulene isomers **TAz2**–**TAz4** are shown in Scheme 1. 2-Chloroazulene-6-boronic acid ester **1**, which is a valuable synthetic intermediate for selective substitution at the 2- and 6-positions in the azulene moiety, was synthesized according to our previous report.[38] Suzuki–Miyaura cross-coupling of **1** with 2-iodoazulene **2** or 6-bromoazulene **3** afforded the 2-chlorobiazulene ester derivatives **4** and **5**, respectively. These derivatives were then treated with 100% phosphoric acid to afford **6** and **7**, respectively. Finally, Suzuki–Miyaura cross-coupling reaction of **6** with 2-azulenyl boronic acid ester **8** gave **TAz2**. **TAz3** and **TAz4** were readily obtained via the Suzuki–Miyaura cross-coupling reactions between **7** and **8** and between **7** and 6-azulenyl boronic acid ester **9**, respectively. All isomers were dark-green crystals and insoluble in common organic solvents such as chloroform, THF, and toluene at room temperature. **TAz2**–**TAz4** were thereby fully characterized by elemental analysis and single-crystal X-ray analysis. Thermogravimetric analysis (TGA) demonstrated that the all of the terazulene isomers exhibit high thermal stability, with a temperature of 5% weight loss greater than 410 °C under nitrogen (see the Supporting Information for TGA analysis,

Scheme 1. Synthesis of TAz2–TAz4 via Suzuki–Miyaura Cross-Coupling

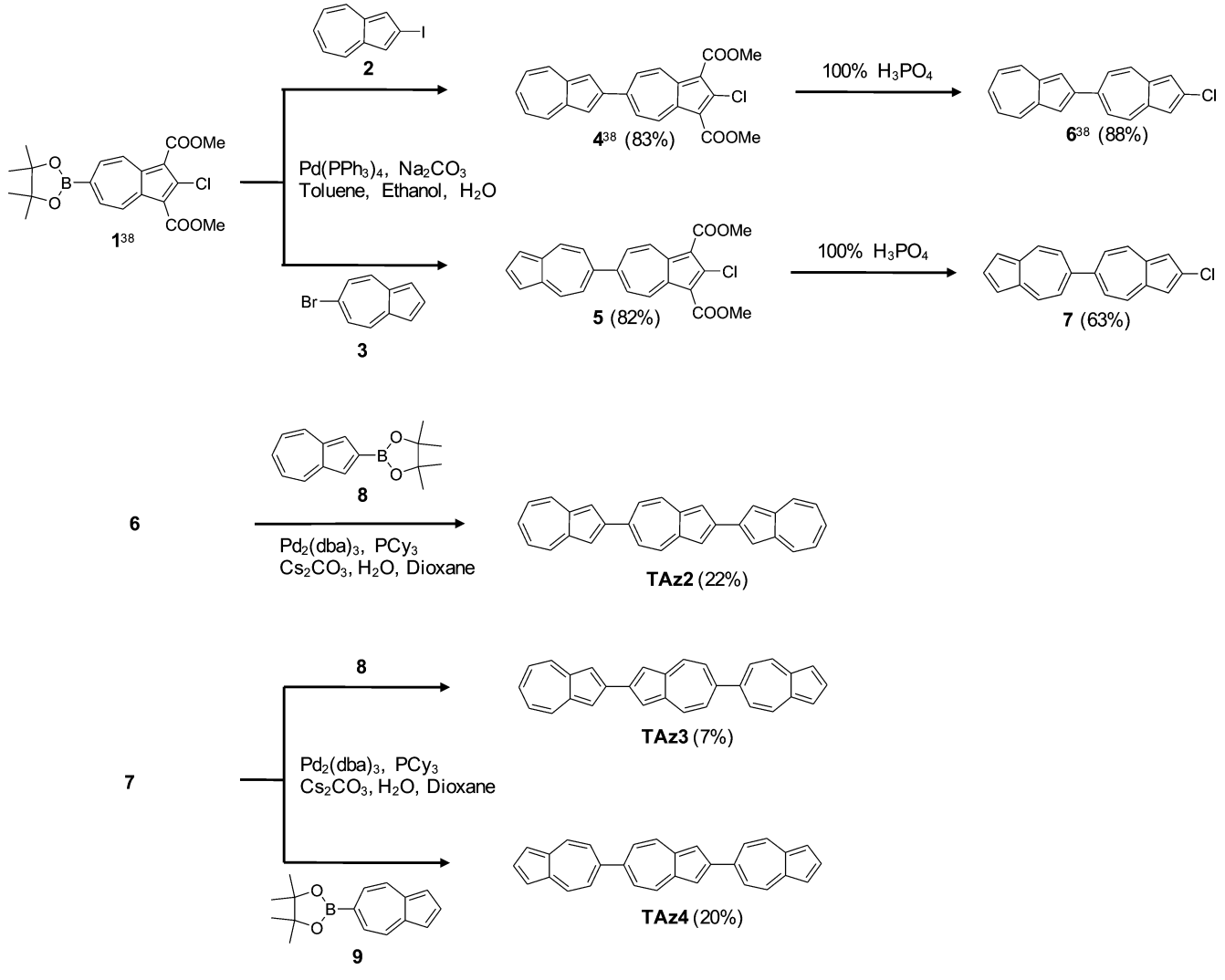

DOI: 10.1021/jacs.6b06877
J. Am. Chem. Soc. 2016, 138, 11335–11343

Figure S16); hence, thermal decomposition of the azulene skeleton would not occur below that temperature.

Optical and Electrochemical Properties. The optical bandgaps and HOMO−LUMO energy levels of the investigated terazulene isomers **TAz2**−**TAz4** were estimated on the basis of UV−vis absorption spectra in thin-film form and photoemission yield spectroscopy (PYS) measurements in air. The results are shown in Figure 2 and Table 1 with the previous data of **TAz1**.[38] All four terazulene isomers exhibited a long-wavelength absorption peak at approximately 600−800 nm (Figure 2a). These results indicate that π-conjugation can be extended in oligoazulene systems when connected at the 2- and 6-positions, irrespective of the direction of the azulene units in the terazulene framework. The lowest transition energies ($E_{g\text{-}abs}$) of **TAz1**−**TAz4** in thin-film form, as estimated from the onset of the film absorptions, are 1.63, 1.62, 1.57, and 1.56 eV, respectively. Notably, all of the terazulene isomers have a fairly narrow bandgap despite the absence of any hetero atoms and electron-donating or -accepting substituents. The HOMO levels of **TAz1**−**TAz4** determined by photoelectron yield spectroscopy were −5.56, − 5.45, − 5.47, and −5.49 eV, respectively, indicating that all of the terazulenes have a sufficiently deep HOMO level to be air stable. In fact, no substantial degradation or decomposition of these compounds was observed even after long-term (approximately 1 year) storage under laboratory ambient conditions. The LUMO level calculated by the addition of the $E_{g\text{-}abs}$ to HOMO levels were −3.93, − 3.83, − 3.90, and −3.93 eV, respectively. The LUMO level of **TAz2** is slightly higher than those of the other isomers.

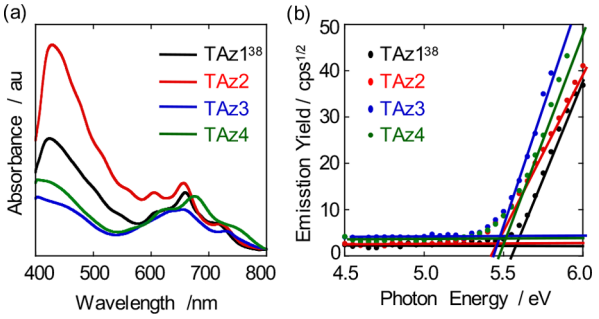

Figure 2. (a) UV−vis absorption spectra of **TAz1**−**TAz4** in thin-film form. (b) Photoemission yield spectra of **TAz1**−**TAz4** in air.

Table 1. Optical Properties of Terazulene Isomers in Thin-Film Form

compound	λ_{onset} (nm)	$E_{g\text{-}abs}$ (eV)[a]	HOMO (eV)[b]	LUMO (eV)[c]
TAz1[38]	757	1.63	−5.56	−3.93
TAz2	764	1.62	−5.45	−3.83
TAz3	785	1.57	−5.47	−3.90
TAz4	795	1.56	−5.49	−3.93

[a]Determined from the absorption edge. [b]Determined by photoemission yield spectroscopy (PYS). [c]LUMO energy levels calculated by the addition of the optical band gap ($E_{g\text{-}abs}$) to the HOMO level.

Crystal Structure Analysis. Single crystals of **TAz2**−**TAz4** were obtained by slow gradient sublimation, and their crystal structures were subsequently determined by single-crystal X-ray analysis. The crystal structures of **TAz2**−**TAz4** are shown in Figure 3 with the previous data of **TAz1**.[38] **TAz1** and **TAz2** showed a rigid and planar molecular structure (Figure 3a,b). As a result, both molecules with an azulene unit connected at the 2,2′- or 2,6′-position should exhibit less hindrance between adjacent azulene moieties. The molecular long axes (*c*-axes) exhibited a layer structure in both crystals (Figure 3a,b), which took the form of well-defined herringbone packing structures typical of edge-to-face stacking. In both crystal structures, structural refinement yielded a global pseudosymmetry with 1:1

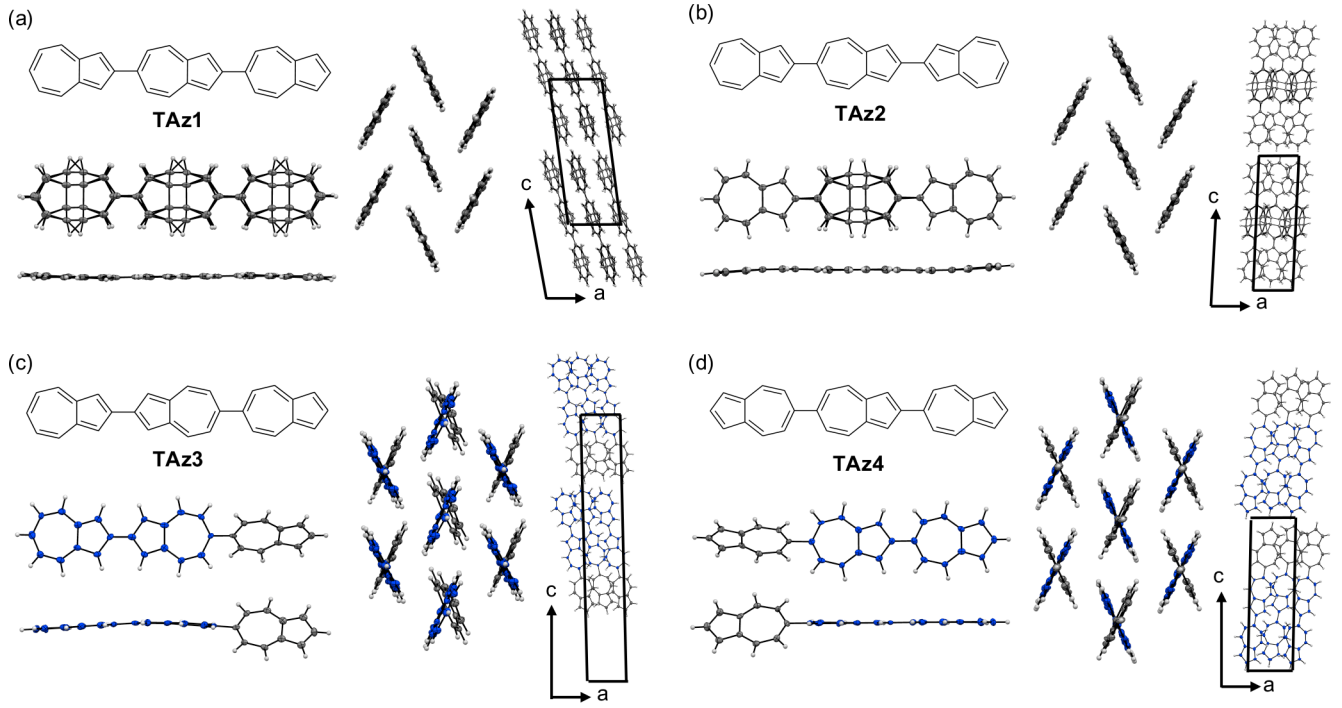

Figure 3. Crystal structures of **TAz1** (a),[38] **TAz2** (b), **TAz3** (c), and **TAz4** (d): Thermal ellipsoid drawing of top and side views at the 50% probability level, partial view along the *b*-axis with clear indication of the layer structure along the *c*-axis, and perspective view with clear indication of the herringbone packing.

DOI: 10.1021/jacs.6b06877
J. Am. Chem. Soc. 2016, 138, 11335−11343

Table 2. OFET Characteristics of the Terazulene Isomers

compound	electrode	T_{sub} (°C)[a]	polarity	μ_{FET_h} ($cm^2\ V^{-1}\ s^{-1}$)	μ_{FET_e} ($cm^2\ V^{-1}\ s^{-1}$)
TAz1	Au[38]	RT	n		1.4×10^{-2}
		60	n		0.11
		100	n		0.29
	Al	RT	n		3.2×10^{-2}
		60	n		0.11
		100	n		0.12
TAz2	Au	RT	p	0.26	
		60	p	0.92	
		100	p	1.32	
	Al	RT	p	0.34	
		60	p	0.86	
		100	ambipolar	7.7×10^{-2}	4.3×10^{-2}
TAz3	Au	RT	ambipolar	7.0×10^{-3}	6.3×10^{-3}
		60	n		0.22
		100	n		0.28
	Al	RT	n		1.9×10^{-3}
		60	n		0.19
		100	n		0.31
TAz4	Au	RT	n		7.3×10^{-2}
		60	n		0.15
		100	n		0.15
	Al	RT	n		7.3×10^{-2}
		60	n		0.15
		100	n		0.15

[a]RT = room temperature.

disorder between the parallel and antiparallel orientations; the two molecules were geometrically equal (Table S1). By contrast, **TAz3** and **TAz4** molecules exhibited a large torsion angle between the seven-membered rings with an azulene unit connected at the 6,6′-position. The dihedral angles between the seven-membered rings in **TAz3** and **TAz4** are 48.5 and 48.7°, respectively (Figure 3c,d). These dihedral angles are mainly attributed to high hindrance between adjacent seven-membered rings in the terazulenes. Interestingly, in the similar case of **TAz1** and **TAz2**, the molecular long axes (*c*-axes) exhibited a lamellar structure (Figure 3c,d), which took the form of the well-defined herringbone arrangement regardless of the twisted molecular configuration. In addition, no disorder was observed between the parallel and antiparallel orientations in any of the crystal structures.

OFET Device Fabrication and Evaluation. Top-contact field-effect transistors were fabricated by vacuum deposition of **TAz1**−**TAz4** on substrates of octadecyl trichlorosilane (ODTS)-treated Si/SiO_2 (300 nm thick thermal SiO_2 on a Si wafer). The source and drain electrodes were deposited by evaporation of gold or aluminum; the channel length and width of the electrodes were 50 μm and 5.5 mm, respectively. The performance of the OFET devices fabricated at different substrate temperature (T_{sub}) was evaluated with the devices in a glovebox; the results are summarized in Table 2. The typical output and transfer curves of the devices were presented in Figure 4. All **TAz1**-based devices exhibited pure typical n-channel field-effect transistor (FET) characteristics irrespective of whether gold or aluminum electrodes were used. The FET mobilities gradually improved with increasing T_{sub}, and the devices fabricated at T_{sub} = 100 °C with gold electrodes demonstrated an electron carrier mobility (μ_{FET}) as high as 0.29 $cm^2\ V^{-1}\ s^{-1}$.[38] Interestingly, all **TAz2**-based devices with gold electrodes exhibited typical p-channel FET characteristics, with μ_{FET_h} = 1.32 $cm^2\ V^{-1}\ s^{-1}$ at T_{sub} = 100 °C, indicating that the polarity completely changed with the direction of the azulene unit. Moreover, **TAz2**-based devices with aluminum electrodes exhibited both p- and n-operation, with a well-balanced mobility of $\mu_{FET\_h} = 7.7 \times 10^{-2}$ $cm^2\ V^{-1}\ s^{-1}$ and $\mu_{FET\_e} = 4.3 \times 10^{-2}$ $cm^2\ V^{-1}\ s^{-1}$ at T_{sub} = 100 °C; thus, **TAz2** clearly exhibits ambipolar character. The pure p-type (no n-type) behavior of the **TAz2**-based devices with gold electrodes is attributed to its LUMO level, which is slightly higher than that of the other terazulene isomers (*vide supra*). All **TAz3**-based devices with gold electrodes exhibited typical n-channel FET characteristics, and the device fabricated at T_{sub} = RT clearly showed both p- and n-type characteristics, with mobilities of $\mu_{FET\_h} = 6.3 \times 10^{-3}$ $cm^2\ V^{-1}\ s^{-1}$ and $\mu_{FET\_e} = 7.0 \times 10^{-3}$ $cm^2\ V^{-1}\ s^{-1}$, respectively. Although the reason why ambipolar performance of **TAz3** was observed only at T_{sub} = RT is unclear at this stage, these results indicate that **TAz3** like **TAz2** has an ambipolar nature. All **TAz4**-based devices showed only n-channel FET characteristics, irrespective of whether gold or aluminum electrodes were used. The devices fabricated at T_{sub} = 60 and 100 °C demonstrated electron carrier mobilities as high as μ_{FET} = 0.15 $cm^2\ V^{-1}\ s^{-1}$.

Thus, overall, **TAz1** and **TAz4** acted as n-type materials in OFETs, whereas **TAz2** and **TAz3** behaved as ambipolar materials in OFETs. These results suggest that terazulene isomers are versatile materials with tunable-polarity FET characteristics that are dependent on the direction of the azulene units in the terazulene backbone. For additional thin-film and device characterization information, see Figures S17−S20.

Thin-Film Microstructural Characterization. To clarify the thin-film morphology of the **TAz1**−**TAz4** films for FET devices with top-contact configuration, atomic force microscopy (AFM) was carried out. The AFM images of the **TAz1**−

DOI: 10.1021/jacs.6b06877
J. Am. Chem. Soc. 2016, 138, 11335−11343

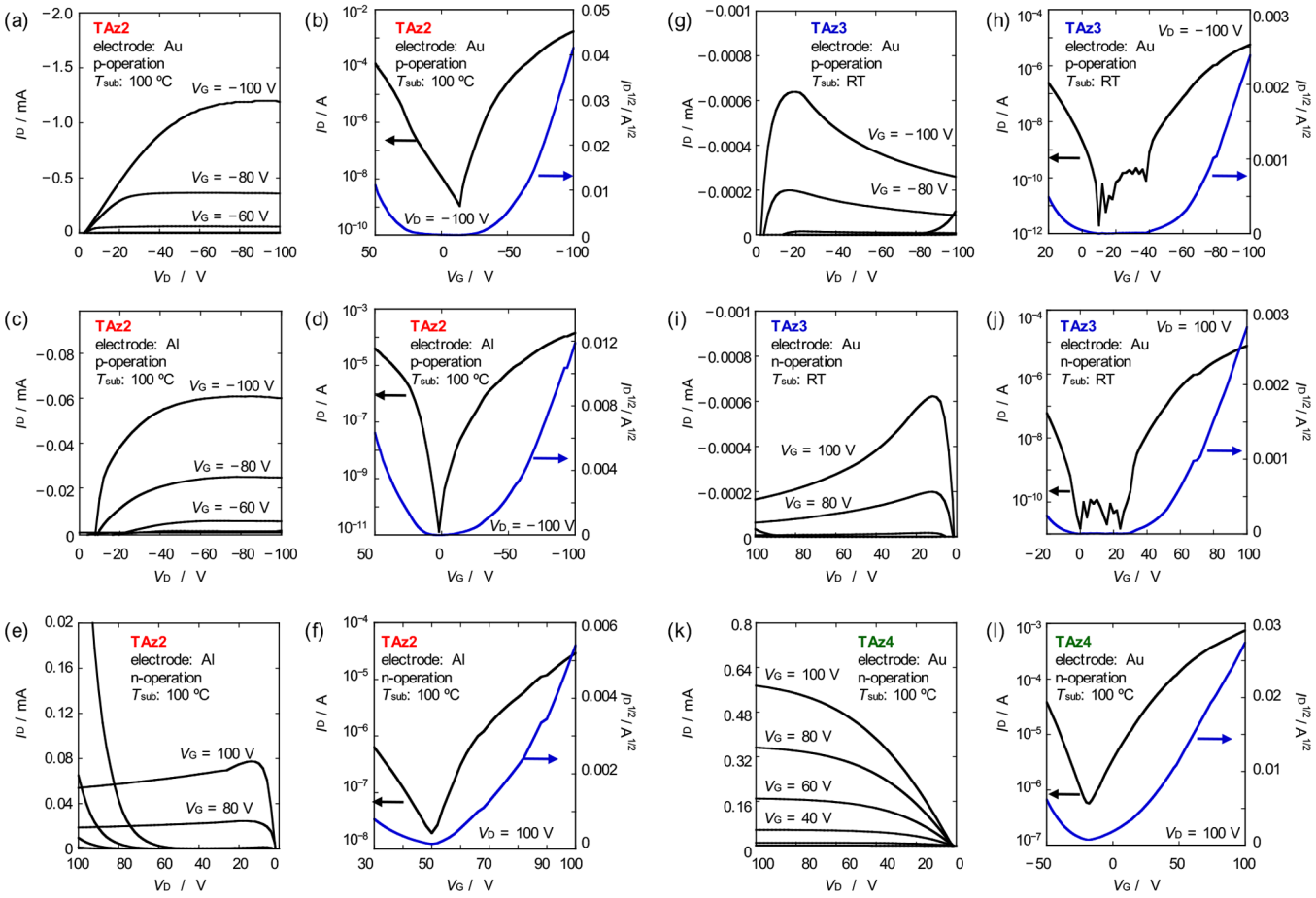

Figure 4. Typical OFET characteristics of top-contact devices fabricated using **TAz2** (a–f), **TAz3** (g–j), and **TAz4** (k and i). (a, c, e, g, i, and k) Output curves at different gate voltages. (b, d, f, h, j, and l) Transfer curves in the saturated region.

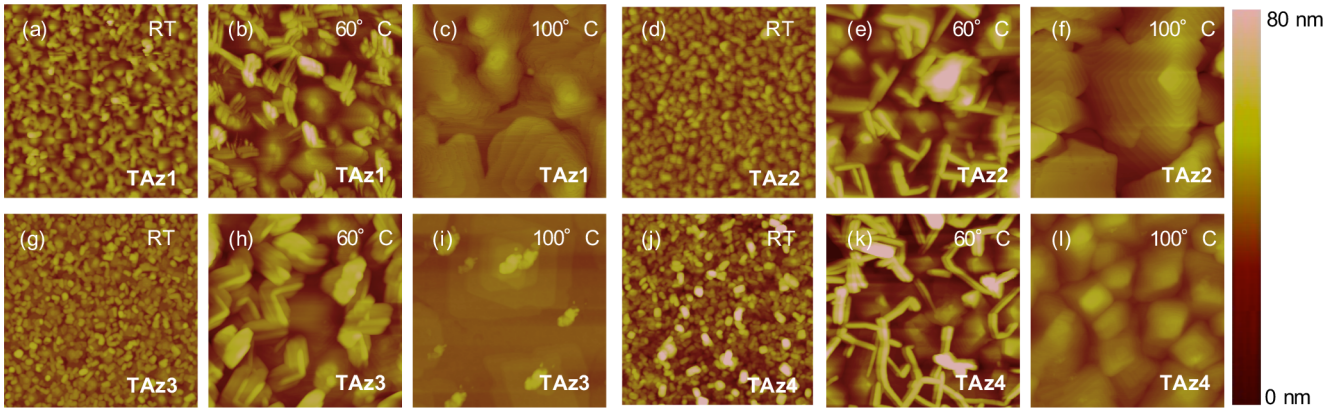

Figure 5. AFM analysis of evaporated thin films of **TAz1**–**TAz4** deposited onto ODTS-treated Si/SiO_2 substrates at different substrate temperatures: **TAz1** (a–c),[38] **TAz2** (d–f), **TAz3** (g–i), and **TAz4** (j–l).

TAz4 films at different T_{sub} are shown in Figure 5. The grain size and regularity of the **TAz1**–**TAz4** films on the substrates were largely influenced by T_{sub}. The **TAz1**–**TAz4** films deposited at T_{sub} = RT showed small grains (Figure 5a,d,g,j). The grains of **TAz1**–**TAz4** were clearly larger in the thin films deposited at T_{sub} = 60 °C, and terrace structures appeared in spots in the thin films (Figure 5b,e,h,k). By contrast, a highly regular terrace structure was observed at T_{sub} = 100 °C in all of the **TAz1**–**TAz4** films (Figure 5c,f,i,l).[39]

The crystal structures of these thin films were analyzed by grazing-incidence X-ray diffraction (GIXD) using synchrotron radiation. Figure 6 displays the 2D GIXD images of the thin films of **TAz1**–**TAz4** fabricated at different temperatures. The 2D GIXD patterns for all of the terazulene isomers were observed as spots, which indicates that these films were highly crystalline; the 2D GIXD patterns gradually improved with increasing T_{sub} and eventually gave numerous sharp reflection spots along q_z (out-of-plane direction) for a given q_{xy} (in-plane direction) at T_{sub} = 100 °C. Moreover, remarkable similarity

DOI: 10.1021/jacs.6b06877
J. Am. Chem. Soc. 2016, 138, 11335–11343

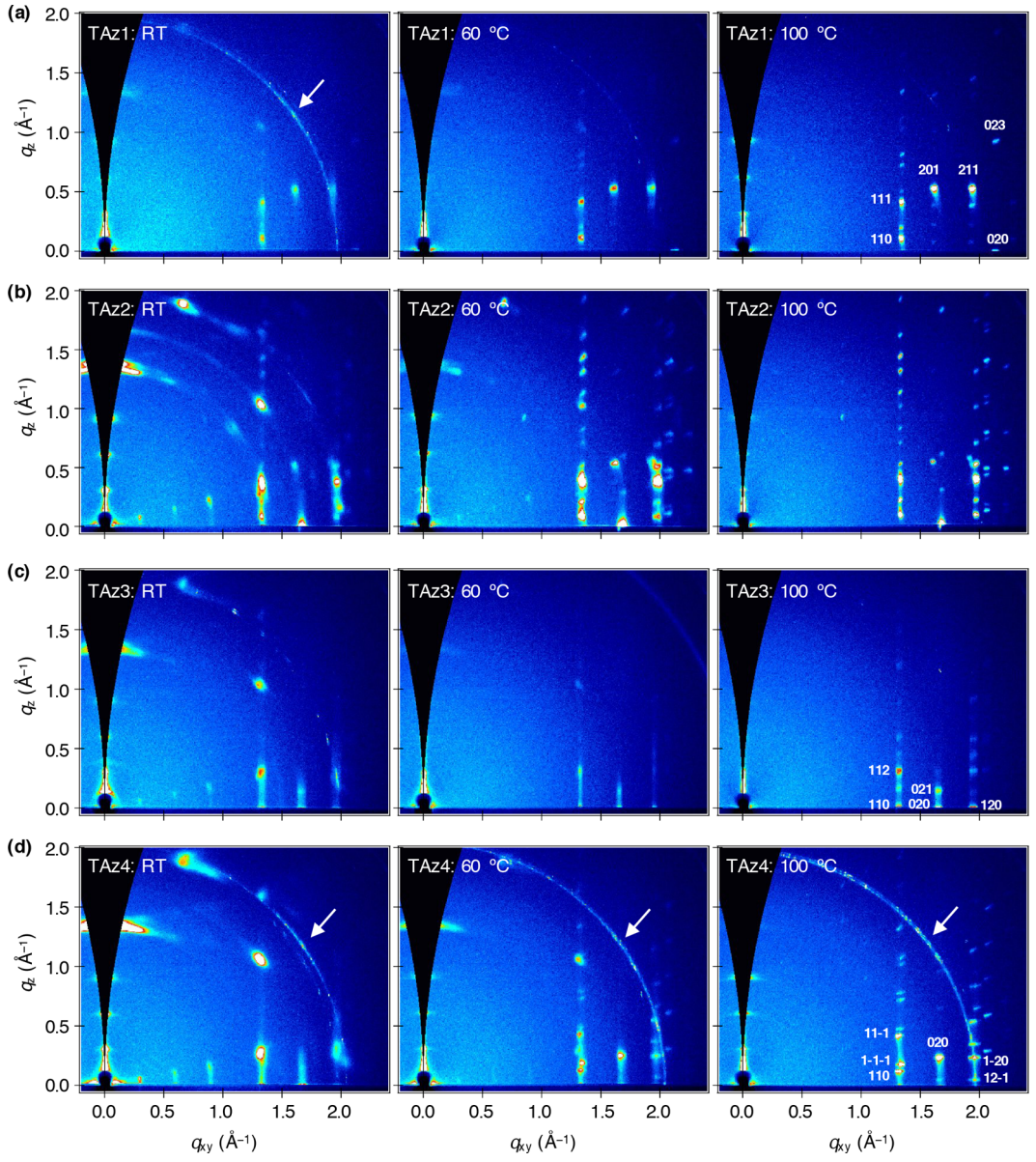

Figure 6. 2D GIXD images of evaporated thin films of **TAz1** (a), **TAz2** (b), **TAz3** (c), and **TAz4** (d) deposited onto ODTS-treated Si/SiO_2 substrates at different substrate temperatures. The Miller indices (*hkl*) were assigned on the basis of the single-crystal data. Artifacts originating from the Si substrate are indicated by white arrows.

was observed between the 2D GIXD pattern and the pattern calculated on the basis of the single-crystal X-ray data; these results indicate that the **TAz1**−**TAz4** molecules stand nearly perpendicular to the ODTS-treated Si/SiO_2 substrate (edge-on orientation) in film form. In **TAz1**, **TAz3**, and **TAz4**, the Miller indices (*hkl*) were assigned on the basis of the single-crystal data (see Supporting Information for experimental details; Figure S21). However, in the case of **TAz2**, Miller indices were not assigned because another similar structure coexisted in the film, similar to the relationship between a bulk phase and a thin-film phase in pentacene thin-film form.[40] In the case of the **TAz1** thin film, little difference was observed in the diffraction patterns obtained at different temperatures, and the reflections became clean, sharp spots with increasing T_{sub}. By contrast, the diffraction pattern of the thin film of **TAz2**−**TAz4** prepared at RT included a small arc pattern, and the diffractions corresponding to the lamellar structure appeared along both the q_z and q_{xy} axes, indicating that edge-on and face-on orientations coexisted in the thin films. Importantly, the optimization of T_{sub} strongly influenced the morphology and resulted in a well-regulated molecular arrangement in the terazulene thin films. In-house XRD measurements also indicated a well-defined crystalline character of **TAz1**−**TAz4** thin films. The out-of-plane XRD patterns showed a series of peaks clearly assignable to (00*h*) reflections, and the in-plane XRD patterns of all of the terazulene isomers clearly showed three typical peaks assignable as π-stacking orientations [(11L), (02L), (12L)] associated with the herringbone structures (see Supporting Information for experimental details; Figure S22).

Theoretical Comparative Studies of Frontier Molecular Orbitals. Density functional theory (DFT) structural optimizations were carried out using the single-crystal X-ray structures with the dihedral angles fixed between the azulene units. Notably, **TAz3** and **TAz4** molecules exhibited a large torsion angle at the 6,6′-position; nevertheless, these LUMOs were overlapped between the 6,6′-bonds, clearly indicating that

DOI: 10.1021/jacs.6b06877
J. Am. Chem. Soc. 2016, 138, 11335−11343

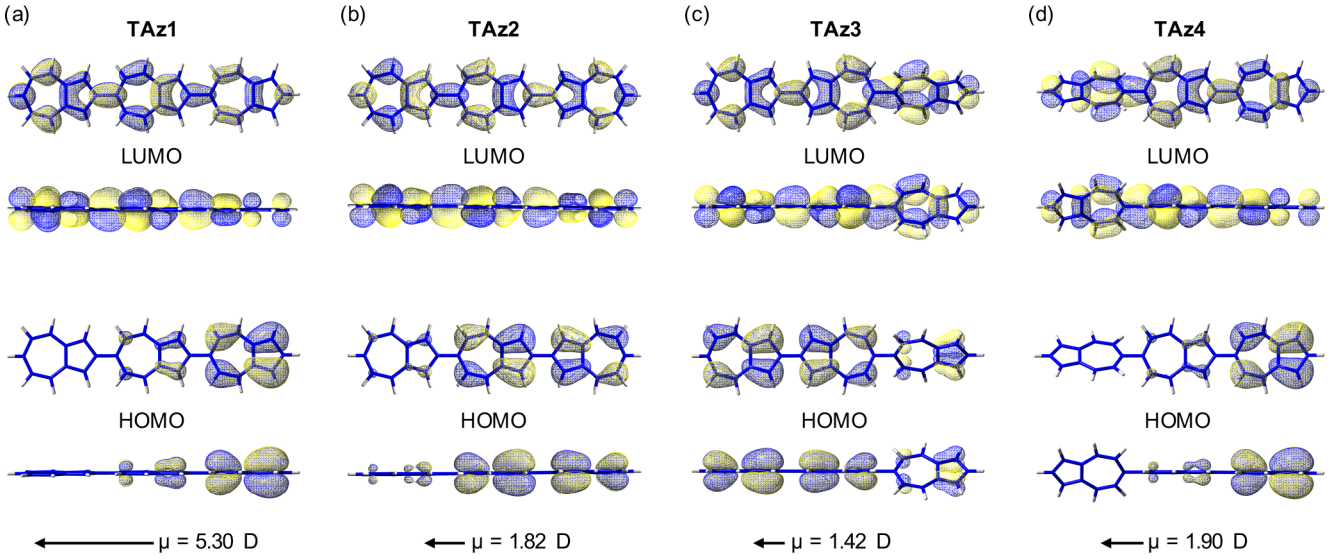

Figure 7. Frontier orbitals and dipole moments of **TAz1** (a), **TAz2** (b), **TAz3** (c), and **TAz4** (d) calculated at the B3LYP/6-31G(d) level: 3D mesh images of the HOMO and LUMO in top view and side view, respectively. The two dihedral angles of azulene planes were fixed during structure optimization at the angles determined from refinement of the crystal structures.

the π-conjugation system is retained in **TAz3** and **TAz4**. The HOMOs of **TAz1** and **TAz4** are substantially localized mainly in the five-membered ring at one end of the azulene moiety, whereas their LUMOs are delocalized and spread over the entire molecule (Figure 7a,d). Therefore, the HOMO cannot overlap adjacent molecules, and hole transport through the crystal is naturally prevented. By contrast, the LUMOs of **TAz1** and **TAz4** can overlap adjacent molecules. Thereby, these compounds favor n-type-specific transport behavior over hole carrier transport. The HOMOs of **TAz2** are mainly spread over the two azulene units in the terazulene backbone, and the LUMO is delocalized over the entire molecule (Figure 7b). As a consequence, both the HOMO and LUMO can overlap adjacent molecules, which explains why **TAz2** exhibits ambipolar character in the OFET device. In the case of **TAz3**, both the HOMO and LUMO coefficients are delocalized, spread over the entire molecule, and capable of overlapping adjacent molecules (Figure 7c). These findings strongly suggest that **TAz3** exhibits ambipolar character in the OFET device.

The unique molecular orbital distribution in terazulene isomers is interpreted as follows, consistent with our previous report.[38] The LUMO of azulene itself displays high orbital density at the 2- and 6-positions, which reveals the strong conjugation between three azulene LUMOs in terazulenes. Consequently, the LUMO of terazulenes has a uniform and broad distribution through the molecule. By contrast, the HOMO of azulene itself has no orbital density at the 2- and 6-positions, which leads to weak conjugation between the three HOMOs; consequently, the three highest orbitals in terazulene generated from three azulene HOMOs closely reflect the distribution of each single azulene unit. In the absence of conjugation, these three orbitals would degenerate and be equally occupied. However, terazulene has a dipole moment (Figure 7), which results in an electrostatic potential gradient inside the molecule and resolves the degeneracy. Indeed, in the cases of **TAz1** and **TAz4**, in which the HOMOs are localized at the end of terazulene molecules, the dipole moment resolved the degeneracy; as a result, **TAz1** and **TAz4** displayed strong gradients, with substantial energy gaps between the HOMO and HOMO − 1 of 0.29 eV for **TAz1** and 0.23 eV for **TAz4** (see Supporting Information for calculation details; Figures S23 and S24 and Table S2). By contrast, **TAz2** and **TAz3**, in which the HOMOs are slightly spread over the terazulene molecules, displayed weak gradients, with small energy gaps between the HOMO and HOMO − 2 of 0.16 eV for **TAz2** and the HOMO and HOMO −1 of 0.05 eV for **TAz3**. In particular, the head-to-head flat antiparallel 2,2′-biazulene unit of **TAz2** and **TAz3** cancels the dipole moment of each azulene unit, resulting in degenerate HOMOs; as a result, the HOMOs spread over the biazulene unit, with small energy gaps between them.

In hopping transport theory, a small reorganization energy and high transfer integral favor high carrier mobility.[41] The reorganization energies of holes for **TAz1**−**TAz4** (0.15, 0.13, 0.05, and 0.13 eV) were smaller than those of electrons (0.31, 0.22, 0.28, and 0.38 eV), indicating that the polarity change of FET should be explained not by the reorganization energy but by the orbital distribution (see Supporting Information for calculation details; Figure S25). The transfer integrals for electron transfer were greater than that for hole transfer in **TAz1**, and no significant difference was observed between each transfer integral in **TAz2** and **TAz3**; together, these results indicate that the transfer integrals clearly reflected the differences in polarity of the FET characteristics in **TAz1**-**TAz3**. By contrast, in the case of **TAz4**, which experimentally exhibited only n-type behavior, transfer integrals were observed for both hole and electron transport with the value of 0.09 and 0.05 eV, respectively. Notably, **TAz4** has a noncentrosymmetric structure in the single crystal, wherein the HOMOs overlap. However, it is generally accepted that the crystal grains take the form of an arbitrary *c*-axis inversion (indistinguishable by 2D GIXD) in the thin-film form, wherein the HOMOs do not overlap.

■ CONCLUSIONS

We have successfully developed all four isomers of terazulene. Linear connections at the 2- and 6-positions on the azulene units reveal the structural advantage of herringbone packing and a unique π-conjugation system with an asymmetric

DOI: 10.1021/jacs.6b06877
J. Am. Chem. Soc. 2016, 138, 11335−11343

distribution of molecular orbitals. The LUMOs of all of the terazulene isomers are broadly distributed through the molecule, achieving a high electronic coupling constant and high electron mobility. By contrast, the HOMOs have individual localizations in each terazulene because of their different dipole moments, resulting in different hole mobilities. In fact, **TAz1** and **TAz4** behave only as n-type FETs, whereas **TAz2** and **TAz3** exhibit both p- and n-type characteristics. The combination of azulene units at the 2- and 6-positions results in notable features: The 2,2′-biazulene unit is important for p-type characteristics, and the polarity of an OFET is changed through the molecular orbital distribution. We believe that the concept could be a key approach to constructing a variety of semiconductor materials. Moreover, hitherto the chemistry of azulene has been developed mainly as solution chemistry and a rarely as liquid crystal;[42−44] these findings provide an additional expectation to accelerate the development of the solid-state chemistry of azulene.

■ ASSOCIATED CONTENT

Supporting Information

The Supporting Information is available free of charge on the ACS Publications website at DOI: 10.1021/jacs.6b06877.

Synthesis and characterization details, ^{1}H and ^{13}C NMR and HRMS data for all new compounds, TGA Analysis, X-ray crystallographic data, OFET device preparation, thin film X-ray diffraction measurement, and theoretical calculation details (PDF)

Crystallographic file for **TAz2** (CIF)

Crystallographic file for **TAz3** (CIF)

Crystallographic file for **TAz4** (CIF)

■ AUTHOR INFORMATION

Corresponding Author

*kgri7078@yz.yamagata-u.ac.jp

Present Address

K.-i.N.: Department of Material and Life Science Graduate School of Engineering, Osaka University 2−1 Yamada-oka, Suita, Osaka 565-0871, Japan.

Notes

The authors declare no competing financial interest.

■ ACKNOWLEDGMENTS

This work was supported by a Grant-in-Aid for Young Scientist (B) (25870076 to H.K.) from the Ministry of Education, Culture, Sports, Science and Technology (MEXT), and CREST program of the Japan Science and Technology Agency (JST). GIXD experiments were performed at the BL19B2 of SPring-8 with the approval of the Japan Synchrotron Radiation Research Institute (JASRI) (Proposal No. 2015B1769). We acknowledge Mr. Kohtaro Takahashi (NAIST) for technical support in GIXD and Ms. Ayako Sato (A Rabbit Science Japan Co., Ltd.) for measurement of elemental analysis.

■ REFERENCES

(1) Anderson, A. G., Jr.; Steckler, B. M. *J. Am. Chem. Soc.* **1959**, *81*, 4941−4946.

(2) Michl, J.; Thulstrup, E. W. *Tetrahedron* **1976**, *32*, 205−209.

(3) Lemal, D. M.; Goldman, G. D. *J. Chem. Educ.* **1988**, *65*, 923−923.

(4) Kurotobi, K.; Kim, K. S.; Noh, S. B.; Kim, D.; Osuka, A. *Angew. Chem., Int. Ed.* **2006**, *45*, 3944−3947.

(5) Muranaka, A.; Yonehara, M.; Uchiyama, M. *J. Am. Chem. Soc.* **2010**, *132*, 7844−7845.

(6) Tang, T.; Lin, T.; Wang, F.; He, C. *Polym. Chem.* **2014**, *5*, 2980−2984.

(7) Wang, F.; Lai, Y.-H.; Kocherginsky, N. M.; Kosteski, Y. Y. *Org. Lett.* **2003**, *5*, 995−998.

(8) Wang, F.; Lai, Y.-H.; Han, M.-Y. *Macromolecules* **2004**, *37*, 3222−3230.

(9) Lacroix, P. G.; Malfant, I.; Iftime, G.; Razus, A. C.; Nakatani, K.; Delaire, J. A. *Chem. - Eur. J.* **2000**, *6*, 2599−2608.

(10) Cristian, L.; Sasaki, I.; Lacroix, P. G.; Donnadieu, B.; Asselberghs, I.; Clays, K.; Razus, A. C. *Chem. Mater.* **2004**, *16*, 3543−3551.

(11) Asato, A. E.; Liu, R. S. H.; Rao, V. P.; Cai, Y. M. *Tetrahedron Lett.* **1996**, *37*, 419−422.

(12) Iftime, G.; Lacroix, P. G.; Nakatani, K.; Razus, A. C. *Tetrahedron Lett.* **1998**, *39*, 6853−6856.

(13) Amir, E.; Amir, R. J.; Campos, L. M.; Hawker, C. J. *J. Am. Chem. Soc.* **2011**, *133*, 10046−10049.

(14) Koch, M.; Blacque, O.; Venkatesan, K. *J. Mater. Chem. C* **2013**, *1*, 7400−7409.

(15) Tsurui, K.; Murai, M.; Ku, S.-Y.; Hawker, C. J.; Robb, M. J. *Adv. Funct. Mater.* **2014**, *24*, 7338−7347.

(16) Ito, S.; Nomura, A.; Morita, N.; Kabuto, C.; Kobayashi, H.; Maejima, S.; Fujimori, K.; Yasunami, M. *J. Org. Chem.* **2002**, *67*, 7295−7302.

(17) Wang, X.; Ng, J. K.-P.; Jia, P.; Lin, T.; Cho, C. M.; Xu, J.; Lu, X.; He, C. *Macromolecules* **2009**, *42*, 5534−5544.

(18) Zhang, X.-H.; Li, C.; Wang, W.-B.; Cheng, X.-X.; Wang, X.-S.; Zhang, B.-W. *J. Mater. Chem.* **2007**, *17*, 642−649.

(19) Puodziukynaite, E.; Wang, H.-W.; Lawrence, J.; Wise, A. J.; Russell, T. P.; Barnes, M. D.; Emrick, T. *J. Am. Chem. Soc.* **2014**, *136*, 11043−11049.

(20) Umeyama, T.; Watanabe, Y.; Miyata, T.; Imahori, H. *Chem. Lett.* **2015**, *44*, 47−49.

(21) Nishimura, H.; Ishida, N.; Shimazaki, A.; Wakamiya, A.; Saeki, A.; Scott, L. T.; Murata, Y. *J. Am. Chem. Soc.* **2015**, *137*, 15656−15659.

(22) Yao, J.; Cai, Z.; Liu, Z.; Yu, C.; Luo, H.; Yang, Y.; Yang, S.; Zhang, G.; Zhang, D. *Macromolecules* **2015**, *48*, 2039−2047.

(23) Murai, M.; Amir, E.; Amir, R. J.; Hawker, C. J. *Chem. Sci.* **2012**, *3*, 2721−2725.

(24) Amir, E.; Murai, M.; Amir, R. J.; Cowart, J. S.; Chabinyc, M. L.; Hawker, C. J. *Chem. Sci.* **2014**, *5*, 4483−4489.

(25) Shevyakov, S. V.; Li, H.; Muthyala, R.; Asato, A. E.; Croney, J. C.; Jameson, D. M.; Liu, R. S. H. *J. Phys. Chem. A* **2003**, *107*, 3295−3299.

(26) Liu, R. S. H.; Asato, A. E. *J. Photochem. Photobiol., C* **2003**, *4*, 179−194.

(27) Shoji, T.; Maruyama, A.; Araki, T.; Ito, S.; Okujima, T. *Org. Biomol. Chem.* **2015**, *13*, 10191−10197.

(28) Clikeman, T. T.; Bukovsky, E. V.; Kuvychko, I. V.; San, L. K.; Deng, S. H. M.; Wang, X.-B.; Chen, Y.-S.; Strauss, S. H.; Boltalina, O. V. *Chem. Commun.* **2014**, *50*, 6263−6264.

(29) Koch, M.; Blacque, O.; Venkatesan, K. *Org. Lett.* **2012**, *14*, 1580−1583.

(30) Murai, M.; Ku, S.-Y.; Treat, N. D.; Robb, M. J.; Chabinyc, M. L.; Hawker, C. J. *Chem. Sci.* **2014**, *5*, 3753−3760.

(31) Anthony, J. E. *Chem. Rev.* **2006**, *106*, 5028−5048.

(32) Desiraju, G. R.; Gavezzotti, A. *Acta Crystallogr., Sect. B: Struct. Sci.* **1989**, *45*, 473−482.

(33) Mei, J.; Diao, Y.; Appleton, A. L.; Fang, L.; Bao, Z. *J. Am. Chem. Soc.* **2013**, *135*, 6724−6746.

(34) Dong, H.; Fu, X.; Liu, J.; Wang, Z.; Hu, W. *Adv. Mater.* **2013**, *25*, 6158−6183.

(35) Wöbkenberg, P. H.; Labram, J. G.; Swiecicki, J.-M.; Parkhomenko, K.; Sredojevic, D.; Gisselbrecht, J.-P.; de Leeuw, D. M.; Bradley, D. D. C.; Djukic, J.-P.; Anthopoulos, T. D. *J. Mater. Chem.* **2010**, *20*, 3673−3680.

(36) Smits, E. C. P.; Setayesh, S.; Anthopoulos, T. D.; Buechel, M.; Nijssen, W.; Coehoorn, R.; Blom, P. W. M.; de Boer, B.; de Leeuw, D. M. *Adv. Mater.* **2007**, *19*, 734−738.
(37) Yamaguchi, Y.; Maruya, Y.; Katagiri, H.; Nakayama, K.-I.; Ohba, Y. *Org. Lett.* **2012**, *14*, 2316−2319.
(38) Yamaguchi, Y.; Ogawa, K.; Nakayama, K.-I.; Ohba, Y.; Katagiri, H. *J. Am. Chem. Soc.* **2013**, *135*, 19095−19098.
(39) Liu, J.; Dong, H.; Wang, Z.; Ji, D.; Cheng, C.; Geng, H.; Zhang, H.; Zhen, Y.; Jiang, L.; Fu, H.; Bo, Z.; Chen, W.; Shuai, Z.; Hu, W. *Chem. Commun.* **2015**, *51*, 11777−11779.
(40) Yoshida, H.; Inaba, K.; Sato, N. *Appl. Phys. Lett.* **2007**, *90*, 181930−181934.
(41) Brédas, J.-L.; Beljonne, D.; Coropceanu, V.; Cornil, J. *Chem. Rev.* **2004**, *104*, 4971−5004.
(42) Adachi, T.; Yamamura, Y.; Hishida, M.; Ueda, M.; Ito, S.; Saito, K. *Liq. Cryst.* **2012**, *39*, 1340−1344.
(43) Adachi, T.; Saitoh, H.; Yamamura, Y.; Hishida, M.; Ueda, M.; Ito, S.; Saito, K. *Bull. Chem. Soc. Jpn.* **2013**, *86*, 1022−1027.
(44) Estdale, S. E.; Brettle, R.; Dunmur, D. A.; Marson, C. M. *J. Mater. Chem.* **1997**, *7*, 391−401.

DOI: 10.1021/jacs.6b06877
J. Am. Chem. Soc. 2016, 138, 11335−11343